Letter Vol. 7, No. 9 / September 2020 / Optica 1093

optica

Hybrid phase-matching for optical parametric amplification of few-cycle infrared pulses

ENRICO RIDENTE,[1,2] MATTHEW WEIDMAN,[1,2,4] MIKHAIL MAMAIKIN,[1,2] CLEMENS JAKUBEIT,[1,2] FERENC KRAUSZ,[1,2] AND NICHOLAS KARPOWICZ[1,3,5]

[1]Max-Planck-Institut für Quantenoptik, Hans-Kopfermann-Strasse 1, 85748 Garching, Germany
[2]Fakultät für Physik, Ludwig-Maximilians-Universität, Am Coulombwall 1, 85748 Garching, Germany
[3]CNR NANOTEC Institute of Nanotechnology, via Monteroni, 73100 Lecce, Italy
[4]e-mail: matthew.weidman@mpq.mpg.de
[5]e-mail: nicholas.karpowicz@nanotec.cnr.it

Received 14 April 2020; revised 17 June 2020; accepted 9 July 2020 (Doc. ID 395265); published 25 August 2020

Simple and compact laser systems facilitate the stable and reproducible generation of high-power few-cycle laser pulses. We demonstrate the amplification of 15 fs pulses at 2.1 μm, employing a hybrid phase-matching scheme for optical parametric chirped pulse amplification. A combination of two BBO crystals with type-I and type-II phase-matching placed in close vicinity is utilized as a single amplification stage. This allows for a greatly simplified layout, achieving high conversion efficiency while avoiding the backconversion regime and the associated spatiotemporal distortions. The resulting system yields mJ-level pulses with integrated electro-optic sampling to directly measure the output waveform and study ultrafast light–matter interaction.

https://doi.org/10.1364/OPTICA.395265

The quest for control of electron motion in atoms, molecules, and solids, as well as a better understanding of their dynamics, has motivated technology development in the area of ultrashort laser pulse generation [1–3]. These achievements have pushed the limits for the shortest possible laser pulses and have led to the generation of isolated attosecond pulses through high harmonic generation (HHG) [4]. Optical parametric chirped pulse amplification (OPCPA) enables both broad amplification bandwidth and power scalability [5]. Because the photon energy for isolated attosecond pulses from HHG scales with the square of the driving laser wavelength [6], these experiments benefit from OPCPA of near-Fourier-limited longer wavelength pulses [7]. Using OPCPA-based systems with ca. 1.8 μm central wavelength, few-cycle pulses have been used to generate isolated attosecond pulses in the x ray water window [8], some of the shortest attosecond pulses [9], and have enabled attosecond experiments [10]. Different OPCPA configurations have been developed to amplify pulses in the IR spectral region [11–13], both at low [14] and high repetition rate [15,16], showing the versatility and robustness of this technique. Nonlinear OPA has also been demonstrated as a reliable and tunable source in the mid-IR [17–19]. A huge variety of amplifying media has been employed for OPCPA. Some of the most common crystal choices in the IR are KTA [20], $LiNbO_3$ [21,22], BiB_3O_6 [23–26], and beta barium borate (BBO) [27–32]. Here, we present a system able to generate 15 fs pulses at 2.1 μm, based on a new two-BBO-crystal amplification scheme with type-I and type-II phase-matching.

The generation of high-power few-cycle pulses can be achieved only if the gain medium can transfer energy efficiently from the pump pulse to the seed pulse over a wide bandwidth [33]. Amplification can be extremely broadband when the zero-dispersion point (ZDP) of the crystal matches the degeneracy wavelength of the OPA process (i.e., twice the pump wavelength) [34]. $LiNbO_3$ has its ZDP at 1.9 μm, making it an excellent candidate for broadband amplification, especially when periodically poled $LiNbO_3$ (PPLN) is used, due to the high effective nonlinearity. However, $LiNbO_3$ is susceptible to photorefraction already at relatively low power densities. We, therefore, use it only in the first amplification stage, as the day-to-day mode modifications, introduced by photorefraction, can cause severe difficulties in experiments making use of the amplified beam.

Instead of BiB_3O_6 or $LiNbO_3$, as previously used [14], two types of BBOs have been combined for the final stage of the OPCPA, which is the stage most responsible for the final bandwidth and conversion efficiency. BBO is a negative uniaxial crystal and has its ZDP at 1.5 μm, resulting in significant negative dispersion in the 2 μm region. Therefore, it might not seem a good candidate, especially considering its significantly smaller nonlinear coefficient. Indeed, the phase-matching bandwidth of a single type-I BBO crystal is significantly narrower for the same gain. However, BBO can phase-match in multiple configurations. This includes the type-I degenerate configuration, more typical of broadband amplification, with signal and idler on the ordinary axis and pump on the extraordinary axis, and a nondegenerate type-II configuration. Here, the signal is on the ordinary axis, and both the pump and idler are on the extraordinary axis. This means that in both types of phase-matching, the relative polarizations of the signal and pump are the same; they differ by the orientation of the idler [Fig. 1(a)].

As the type-II process is nondegenerate, the amplification band is a single peak, whose wavelength can be chosen through the angle θ, whereas the degenerate type-I amplification band has two peaks mirrored around the degeneracy point (which tend to

merge with increased pump intensity). These three features can be made to be nonoverlapping, and thus, energy may be transferred from the same pump to the signal, collinearly in two crystals. The idler produced in the first crystal is inactive in the second crystal because it has the wrong polarization to serve as idler in the type-II process, and it is outside of the phase-matching bandwidth to serve as signal. This effectively resets the saturation of the amplification process, allowing additional energy to be extracted from the pump, while broadening the total amplification bandwidth of the combined stage.

In our system, a laser seed, centered around 2.1 μm, is amplified in two stages: in a PPLN crystal and in two BBO crystals. Within the first BBO (type-I, theta = 21.5°), the low frequency region of the seed spectrum is phase-matched, from 125 THz to 165 THz, whereas within the second BBO (type-II, theta = 29.48°) the higher frequency region is phase-matched, from 165 THz to 187 THz, as shown in a numerical simulation of the nonlinear process [35] in Figs. 1(b) and 1(c). This indicates that a two-crystal BBO amplification stage would exhibit a similar bandwidth compared to a $LiNbO_3$-based stage, with advantages in both the damage threshold of the crystals and reduced photorefraction, and

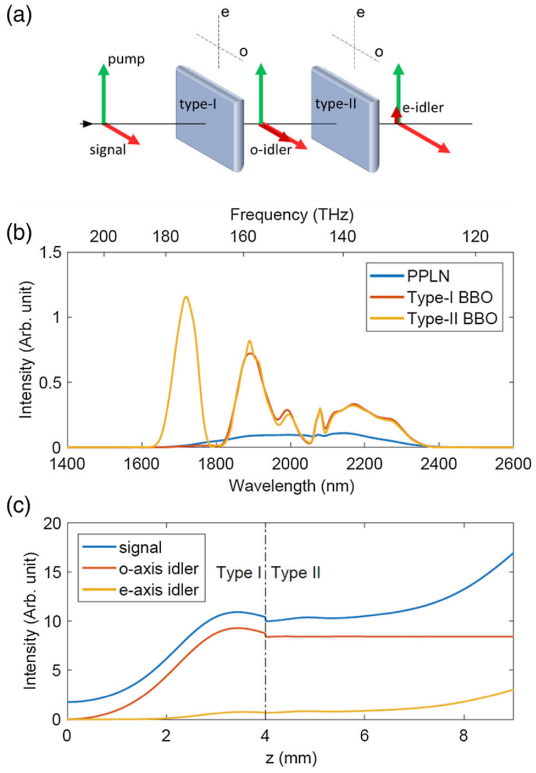

Fig. 1. OPCPA in a two-crystal BBO system is simulated numerically. A super-Gaussian, broadband seed is first amplified in a 1-mm-thick PPLN with a 32.5 μm poling period (stage 1), providing the seed for the two-crystal BBO stage (stage 2). The last stage comprises a 4-mm-thick type-I BBO at theta = 21.5°, and a 5-mm-thick type-II BBO at theta = 29.5°. (a) Phase-matching in the two BBO crystals. (b) Spectra after the first, second, and third crystal. (c) The gain dynamics. Notably, the idler on the *o* axis, produced in the type-I BBO, remains essentially frozen in amplitude as it crosses the second crystal; saturation and the backconversion of the signal and idler into pump that would have occurred if the first crystal was longer are halted, and amplification in the shorter wavelength band begins at $z = 4$ mm, the entrance surface of the second crystal.

a significant suppression of parasitic nonlinear effects that reduce the conversion efficiency of the OPCPA.

An implementation of this concept is shown in Fig. 2. The seed and pump schematic are the same as the ones described in [14]. A Ti:sapphire oscillator (Rainbow II, Femtolasers GmbH) generates broadband pulses carried at a central wavelength of 780 nm. A dichroic beam splitter is used to send the spectral region around 1030 nm to a Yb:YAG thin-disk regenerative amplifier [36]. The outgoing beam has a power of 50 W and a pulse duration of 1.4 ps, after compression. The pulses at 780 nm are amplified in a CPA, and 5% of the output power is broadened in a hollow core fiber (HCF) [37], with the rest of the energy available for other experiments.

The output of the HCF is compressed using chirping mirrors (CMs) and relay imaged onto a 500-μm-thick type-II BBO crystal (Fig. 2) to produce the seed pulses via intrapulse difference frequency generation (DFG) [38]. We use BBO for seed generation as its output demonstrated higher reproducibility and a smoother spectral phase than the MgO-doped PPLN that was used previously [39]. The DFG has a central wavelength of 2.1 μm and a spectrum that extends from 1.5 μm to 2.5 μm [Fig. 3(a)]. Intrapulse DFG passively stabilizes the CEP, making the system suitable for electric-field-sensitive measurements. To record the day-to-day fluctuations, the spectrum was measured 20 times over a period of one month. The standard deviation is shown in the shaded area of Figs. 3(a)–3(c). The broad spectrum supports Fourier transform limited pulses as short as 12 fs, equal to two optical cycles. An advantage of using type-II BBO for generating the 2.1 μm seed pulses, while sacrificing efficiency compared to the type-I process, is that the polarization of the newly generated frequencies is orthogonal to the polarization of the transmitted white light. This means that the two pulses can be simply and cleanly separated using a broadband wire grid polarizer—and ultimately the WL can be recompressed and utilized as a synchronized few-femtosecond probe pulse.

Before being split, both the DFG and the WL beam are recollimated using a 90° off-axis parabolic mirror (OAP). This is the only necessary reflective optic, in addition to three reflective mirrors, used along the 2.1 μm beam path in the OPCPA, making the design of the system particularly simple.

The seed pulses are stretched using a combination of bulk crystals (Si and ZnSe) and in an acousto-optic programmable

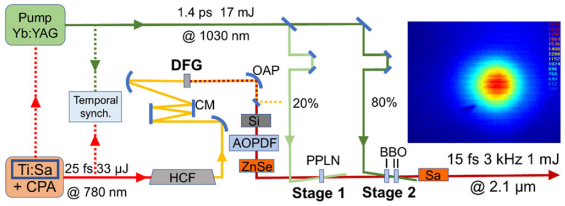

Fig. 2. Ti:Sa generated pulses are split to feed an Yb:YAG disk oscillator and a CPA. The disk amplifier delivers 17 mJ and pumps the two OPCPA stages. 5% of the CPA output is broadened in a hollow core fiber (HCF) and is compressed using chirped mirrors (CMs). Through intrapulse DFG in a BBO crystal, the 2.1 μm OPCPA seed is generated. A 90° off-axis parabola (OAP) recollimates the 2.1 μm beam and the transmitted WL, and a polarizer separates the two. The seed goes through a 1-cm-thick Si bulk, the AOPDF, and 1 cm of ZnSe before being amplified in stage 1, by a PPLN crystal and in stage 2 by the two BBO crystals and compressed in a sapphire block (Sa). After amplification and compression, the pulses have an energy of 1 mJ and a duration of 15 fs. The inset shows the beam mode after amplification.

dispersive filter (AOPDF) to approximately 280 fs FWHM. The AOPDF compensates for dispersion in the Si, ZnSe, PPLN (first OPCPA stage), two BBOs (second OPCPA stage), and the sapphire (Sa). Unlike in [14], where the amplification happened in three stages, here it is performed in two. The first consists of a 1-mm-thick PPLN and is used to amplify the seed to 120 mW [spectrum shown in Fig. 3(b)]. The crystal is pumped with 20% of the Yb:YAG thin-disk laser output power. The pointing of both the pump and seed beams is actively stabilized, and the temporal synchronization is maintained using an active spectrally resolved cross-correlator stabilization system [40]. The second amplification stage consists of a combination of a 4-mm-thick type-I BBO crystal followed by a 5-mm-thick type-II BBO crystal [spectrum shown in Fig. 3(c)]. The two crystals are independently mounted and adjustable; yet, the spacing between them is kept as small as possible, ca. 2 mm. Because they share the same pump beam, the noncollinear angle between the pump and the signal beams is minimized, here approximately 2°. Both BBO crystals have a diameter of 1 cm, larger than commercially available periodically poled $LiNbO_3$ crystals. The BBO stage is pumped with the remaining 80% of the Yb:YAG pump power and provides 3 W average power. Following the amplification in the second stage, the 2.1 μm output pulses are compressed to 15 fs by using a 1-cm-thick sapphire block. The intensity profile of the amplified beam does not show any strong asymmetry as can be seen in the inset of Fig. 2.

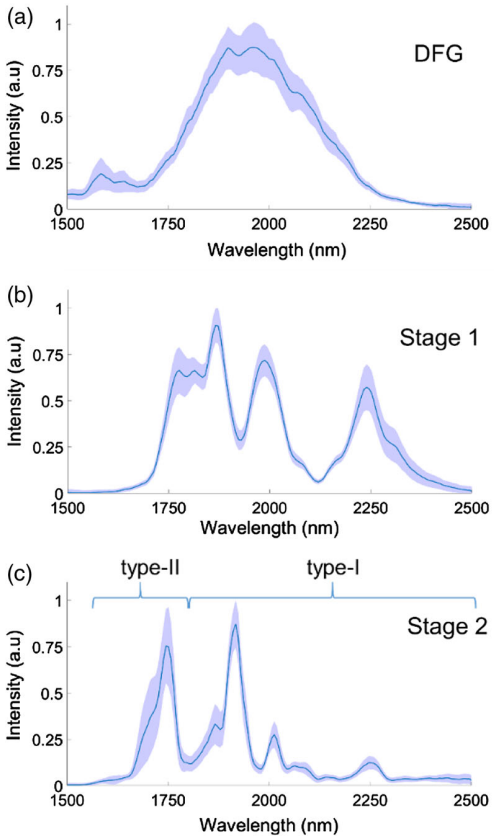

Fig. 3. Spectra averaged over one month of operation: (a) intrapulse DFG, (b) first, and (c) second amplification stage. Solid blue line, the averaged spectrum. Shaded area, the standard deviation of each frequency. The good reproducibility of the spectra demonstrates high stability of the amplified pulses. Curly brackets in (c) show the spectral regions where the two BBOs are phase-matched.

The seed spot size in the two stages has been chosen such that no telescope is needed between the PPLN and the BBOs (0.7 mm and 1.1 mm $1/e^2$, respectively)—in fact, there are no optics in the seed path after the first amplification stage. This implies that the pump beam size must be wisely chosen to maximize the OPCPA efficiency. Telescopes have been implemented in the two pump beam paths, to obtain an optimal spot size of 2.5 mm on the PPLN and 2.3 mm on the BBOs ($1/e^2$). As a result, no telescope is needed between the two stages. This simple two-stage setup has a dramatically shorter beam path compared to the previous system, which is a significant advantage in a spectral region of non-negligible atmospheric absorption [40].

The reported values correspond to the system as optimized for stable and reproducible day-to-day operation. In principle, higher conversion efficiency and output power are possible through reduced pump and seed spot sizes, and increasing the number of amplification stages. Doing this presents a risk of thermal failure of the crystal—operation in such a configuration with 6 W output power caused the final BBO to crack.

The amplified pulses have been measured via electro-optic sampling (EOS). EOS is a field-resolved technique commonly used to characterize terahertz fields [41], which has recently been extended to retrieve pulses with frequencies up to 250 THz [35]. A sampling pulse is needed to retrieve the electric field of the OPCPA pulses (test pulse). In our setup, the sampling pulse is the residual WL from the intrapulse DFG (Fig. 2). CMs are used to compress the pulse to 4 fs, which is afterward recombined with the OPCPA pulses on a second wiregrid polarizer. The sampling and test pulses are focused collinearly on a 100-μm-thick type-II BBO (EOS crystal) phase-matched for sum frequency generation. The change in polarization of the sampling pulse, induced by the spectrally overlapping part of the sum frequency, is measured using an ellipsometer with balanced photodiodes. The difference between the currents of the two photodiodes is proportional to the test pulse electric field at a given time, without the need for an iterative reconstruction algorithm to retrieve the pulse. Heterodyne detection, achieved using a lock-in amplifier referenced to a phase modulation imposed via the AOPDF, improves the signal-to-noise ratio, allowing us to determine the electric field [Fig. 4(a)] in a single scan. Being a field sensitive technique, EOS gives access to the full spectral phase of the pulse. This information can be fed back to the AOPDF to further optimize the pulse compression correcting for higher-order dispersion. The idea behind this optimization process is the following: in theory, a flat spectral phase is wanted to produce Fourier limited pulses. This can be achieved by subtracting from the applied AOPDF phase the one retrieved via EOS, thus producing a compressed pulse at the OPCPA output. After a few iterations, the pulse has a higher peak power and a shorter duration.

When dealing with few-cycle pulses, the CEP plays a crucial role in their characterization, since it defines their asymmetry. The beam after the second amplification stage is sent to an $f-2f$ interferometer based on a second HCF and second harmonic generation in a BBO crystal. The position of the resulting interference fringes is directly related to the CEP. Due to the integration time of the spectrometer, each spectrum is an average of 25 laser shots. The CEP standard deviation is 64.7 mrad over a span of 1 h [Fig. 4(b)]. The value is smaller by a factor of two compared to the previous three-stage version [14], demonstrating the improved stability of the system.

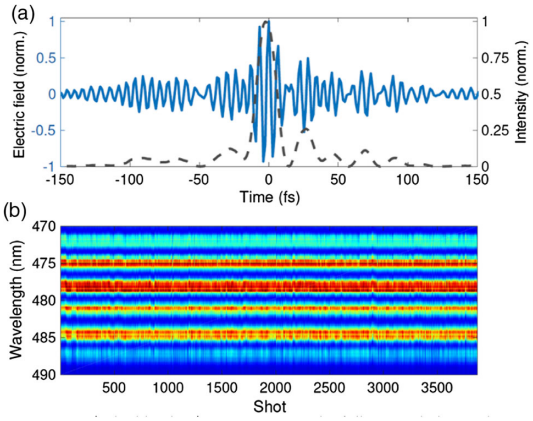

Fig. 4. (a) Reconstructed EOS trace (solid blue line) gives access to the full spectral phase. The OPCPA amplified pulses have a pulse duration of 15 fs with a central wavelength of 2.1 μm. The intensity profile (dashed gray line) shows how most of the pulse energy is confined within few field cycles. Their CEP can be actively controlled using the AOPDF, allowing the study of field sensitive light–matter interaction phenomena. (b) The CEP stability of the pulses has been measured over 1 h with an $f-2f$ interferometer, resulting in a standard deviation of 64.7 mrad.

In conclusion, we presented a new OPCPA configuration capable of amplifying 2.1 μm pulses up to the mJ-level. The combination of two BBO parametric amplifier crystals with type-I and type-II phase-matching results in improved beam quality, amplification stability, and versatility compared to previous $LiNbO_3$-based OPCPA systems.

Funding. Air Force Office of Scientific Research (FA9550-15-1-0037, FA9550-16-1-0073); Army Research Office (W911NF-15-1-0360); Horizon 2020 Framework Programme (EU-H2020 654148).

Acknowledgment. The authors thank H. Fattahi for the helpful discussions and O. Razskazovskaya and Y.-L. Li for their help in the laboratory.

Disclosures. The authors declare no conflicts of interest.

See Supplement 1 for supporting content.

REFERENCES

1. M. Hentschel, R. Kienberger, C. Spielmann, G. A. Reider, N. Milosevic, T. Brabec, P. Corkum, U. Heinzmann, M. Drescher, and F. Krausz, Nature **414**, 509 (2001).
2. M. Y. Ivanov, R. Kienberger, A. Scrinzi, and D. M. Villeneuve, J. Phys. B **39**, 1 (2005).
3. F. Krausz and M. Ivanov, Rev. Mod. Phys. **81**, 163 (2009).
4. S. Gholam-Mirzaei, J. Beetar, and M. Chini, Appl. Phys. Lett. **110**, 061101 (2017).
5. H. Fattahi, H. G. Barros, M. Gorjan, T. Nubbemeyer, B. Alsaif, C. Y. Teisset, M. Schultze, S. Prinz, M. Haefner, M. Ueffing, A. Alismail, L. Vámos, A. Schwarz, O. Pronin, J. Brons, X. T. Geng, G. Arisholm, M. Ciappina, V. S. Yakovlev, D.-E. Kim, A. M. Azzeer, N. Karpowicz, D. Sutter, Z. Major, T. Metzger, and F. Krausz, Optica **1**, 45 (2014).
6. A. D. Shiner, C. Trallero-Herrero, N. Kajumba, H. C. Bandulet, D. Comtois, F. Légaré, M. Giguère, J. C. Kieffer, P. B. Corkum, and D. M. Villeneuve, Phys. Rev. Lett. **103**, 073902 (2009).
7. B. Shan and Z. Chang, Phys. Rev. A **65**, 011804 (2001).
8. F. Silva, S. M. Teichmann, S. L. Cousin, M. Hemmer, and J. Biegert, Nat. Commun. **6**, 6611 (2015).
9. J. Li, X. Ren, Y. Yin, K. Zhao, A. Chew, Y. Cheng, E. Cunningham, Y. Wang, S. Hu, and Y. Wu, Nat. Commun. **8**, 186 (2017).
10. C. Zhang, G. Vampa, D. M. Villeneuve, and P. B. Corkum, J. Phys. B **48**, 061001 (2015).
11. A. Mussot, A. Kudlinski, P. B. d'Augères, and E. Hugonnot, Opt. Express **21**, 12197 (2013).
12. O. D. Mücke, D. Sidorov, P. Dombi, A. Pugžlys, S. Ališauskas, V. Smilgevičius, N. Forget, J. Posius, L. Giniūnas, R. Danielius, and A. Baltuška, Opt. Spectrosc. **108**, 456 (2010).
13. C.-H. Lu, T. Witting, A. Husakou, M. J. Vrakking, A. Kung, and F. J. Furch, Opt. Express **26**, 8941 (2018).
14. Y. Deng, A. Schwarz, H. Fattahi, M. Ueffing, X. Gu, M. Ossiander, T. Metzger, V. Pervak, H. Ishizuki, T. Taira, T. Kobayashi, G. Marcus, F. Krausz, R. Kienberger, and N. Karpowicz, Opt. Lett. **37**, 4973 (2012).
15. Z. Heiner, V. Petrov, G. Steinmeyer, M. J. J. Vrakking, and M. Mero, Opt. Express **26**, 25793 (2018).
16. A. Killi, A. Steinmann, G. Palmer, U. Morgner, H. Bartelt, and J. Kobelke, Opt. Lett. **31**, 125 (2006).
17. J. Vogelsang, J. Robin, B. Piglosiewicz, C. Manzoni, P. Farinello, S. Melzer, P. Feru, G. Cerullo, C. Lienau, and P. Groß, Opt. Express **22**, 25295 (2014).
18. O. Isaienko and E. Borguet, J. Opt. Soc. Am. B **30**, 2075 (2013).
19. S. Lochbrunner, T. Wilhelm, J. Piel, S. Sporlein, and E. Riedle, *Advanced Solid State Lasers* (1999), paper TuA4.
20. M. Mero, F. Noack, F. Bach, V. Petrov, and M. J. J. Vrakking, Opt. Express **23**, 33157 (2015).
21. M. Baudisch, A. Thai, M. Hemmer, H. Ishizuki, T. Taira, and J. Biegert, *Advanced Solid-State Lasers Congress* (2013), paper AF1A.7.
22. T. Fuji, N. Ishii, C. Y. Teisset, X. Gu, T. Metzger, A. Baltuska, N. Forget, D. Kaplan, A. Galvanauskas, and F. Krausz, Opt. Lett. **31**, 1103 (2006).
23. N. Ishii, K. Kitano, T. Kanai, S. Watanabe, and J. Itatani, Appl. Phys. Express **4**, 022701 (2011).
24. Y. Yin, J. Li, X. Ren, K. Zhao, Y. Wu, E. Cunningham, and Z. Chang, Opt. Lett. **41**, 1142 (2016).
25. S. Wandel, G. Xu, Y. Yin, and I. Jovanovic, J. Phys. B **47**, 234016 (2014).
26. N. Ishii, K. Kaneshima, K. Kitano, T. Kanai, S. Watanabe, and J. Itatani, Opt. Lett. **37**, 4182 (2012).
27. F. Silva, P. K. Bates, A. Esteban-Martin, M. Ebrahim-Zadeh, and J. Biegert, Opt. Lett. **37**, 933 (2012).
28. C.-J. Lai, K.-H. Hong, J. P. Siqueira, P. Krogen, C.-L. Chang, G. J. Stein, H. Liang, P. D. Keathley, G. Laurent, J. Moses, L. E. Zapata, and F. X. Kärtner, J. Opt. **17**, 094009 (2015).
29. Y. Shamir, J. Rothhardt, S. Hädrich, S. Demmler, M. Tschernajew, J. Limpert, and A. Tünnermann, Opt. Lett. **40**, 5546 (2015).
30. B. E. Schmidt, A. D. Shiner, P. Lassonde, J.-C. Kieffer, P. B. Corkum, D. M. Villeneuve, and F. Légaré, Opt. Express **19**, 6858 (2011).
31. C. Li, D. Wang, L. Song, J. Liu, P. Liu, C. Xu, Y. Leng, R. Li, and Z. Xu, Opt. Express **19**, 6783 (2011).
32. K.-H. Hong, S.-W. Huang, J. Moses, X. Fu, C.-J. Lai, G. Cirmi, A. Sell, E. Granados, P. Keathley, and F. X. Kärtner, Opt. Express **19**, 15538 (2011).
33. C. Schmidt, J. Bühler, A. C. Heinrich, A. Leitenstorfer, and D. Brida, J. Opt. **17**, 094003 (2015).
34. R. Dabu, Opt. Express **18**, 11689 (2010).
35. S. Keiber, S. Sederberg, A. Schwarz, M. Trubetskov, V. Pervak, F. Krausz, and N. Karpowicz, Nat. Photonics **10**, 159 (2016).
36. T. Metzger, C. Y. Teisset, and F. Krausz, *Advanced Solid-State Photonics* (2008), paper TuA2.
37. P. S. J. Russell, P. Hölzer, W. Chang, A. Abdolvand, and J. C. Travers, Nat. Photonics **8**, 278 (2014).
38. H. Fattahi, A. Schwarz, S. Keiber, and N. Karpowicz, Opt. Lett. **38**, 4216 (2013).
39. A. Schwarz, "Few-cycle phase-stable infrared OPCPA," Ph.D. Thesis (LMU, 2014).
40. M. Gebhardt, C. Gaida, F. Stutzki, S. Hädrich, C. Jauregui, J. Limpert, and A. Tünnermann, Opt. Express **23**, 13776 (2015).
41. Q. Wu and X. C. Zhang, Appl. Phys. Lett. **67**, 3523 (1995).